Metallic surface temperature at the very beginning of the laser-induced breakdown obtained from black-body radiation

Miloš Skočić,* Dejan Dojić, and Srdjan Bukvić
University of Belgrade, Faculty of Physics, Studentski Trg 12-16, 11000 Belgrade, Serbia

(Received 27 December 2021; accepted 30 March 2022; published 29 April 2022)

We present experimental results of cooper surface temperature measured nanosecond by nanosecond at the very beginning of the laser-induced breakdown experiment. The experiment is conducted by Nd:YAG laser for three irradiances: 1.4×10^{9}, 3.2×10^{11}, and 3.7×10^{12} W/cm^2. The temperatures of the metal surface, before plasma is created, are in the interval 7 400–11 200 K. These values are close to most estimates for the critical temperature of copper. The moment when plasma was created is recognized applying a bifurcated optical cable. After creation, temperature of the plasma increases attaining values over 50 000 K. All temperatures are derived relying on continuous spectra emitted from the bright spot illuminated by the laser.

DOI: 10.1103/PhysRevE.105.045211

I. INTRODUCTION

Laser-induced plasma (LIP) has been the subject of intensive research in recent decades. It is created by interaction of powerful pulsed lasers with solid targets, liquids, and gaseous media. Depending on laser energy and pulse duration elementary processes taking place during illumination of targets are essentially different. For common nanosecond lasers interacting with metallic targets the process starts with heating of the solid target, followed by melting and evaporation of the target material [1,2]. Due to high temperature the illuminated area of the target becomes bright with dominantly continuous spectrum. The evaporated material expands, absorbs laser radiation, heats up, and becomes a high-density plasma emitting in most cases continuous spectrum [3,4]. Investigating the amount of ablated material some authors consider "phase explosion" as the most relevant process for transition from metallic to gaseous state [2,5–9]. Reported critical temperature, associated to critical point of copper, ranges in a broad interval (5400–8900 K) depending on research methodology which is applied in specific study [10–12].

Estimation of the metallic target temperature during the laser action and onset temperature of the LIP is of interest for experimental characterization of the plasma expansion. Also the temperature of the metallic target while it is illuminated by the laser is an important initial parameter used in different numerical simulations [2,13,14]. In Ref. [4] Bataller *et al.* show that the plasma created in high pressure (5 bar) Xe by 0.12 ps laser pulse radiates as a nearly black body with emissivity $\epsilon \approx 1$ measured with 15% accuracy. The authors report plasma temperatures, immediately after the breakdown, to be about 16 000 K. In Ref. [3] the authors measured attenuation of the He-Ne beam (633 nm) in the copper plasma expanding in vacuum and found that the plasma was partially transparent, despite the pure continuous spectrum similar to radiation of black body. The aim of this work is to measure temperature of area illuminated by the laser, nanosecond by nanosecond, correlating recorded spectrum with black-body radiation.

II. EXPERIMENTAL SETUP

The experimental setup consist of a homemade chamber with high purity flat copper sample placed inside the chamber. The chamber is filed up with residual atmosphere at pressure less than 0.05 mbar. To prevent drilling of the sample chamber is mounted on computer controlled *x*-*y*-*z* translation stage. The plasma was created by a focused laser beam from pulsed Nd:YAG, EKSPLA NL311-SH-TH, laser. Duration of the pulse (fundamental harmonic at 1064 nm wavelength) was 5.6 ns with repetition rate of 1 Hz. The spatial intensity profile of the laser spot on the target's surface had a top-hat form. The diameter of the spot was 0.1 mm. Dispersion system is based on Andor Shamrock SR-163 spectrograph with intensified CCD camera (2048 × 512 pixels) Andor iStar DH740-18F-03, cooled down to −20 °C, as the detection system. The spectral range covered by the CCD chip, in this configuration, is from 200 nm to 850 nm. Bifurcated optical cable is used to simultaneously monitor bright area from the front side and side-on, see Figs. 1 and 2. On both legs of the optical cable are mounted identical SMA collecting lenses focused on the bright spot area generated by the laser. The optical axis of the side-on collecting lens is adjusted to be parallel with sample surface. The both collecting lenses are out of the chamber close to the chamber windows made of fused silica glass. The radiometric calibration (chamber window + collecting lens + optical fiber + CCD) is done relying on deuterium spectral lamp provided by StellarNet for UV and tungsten lamp for visible spectrum. Appropriate set of filters is used to prevent overlapping of the spectra coming from different spectral orders. The laser controller provides trigger signal which precedes actual firing of the Nd:YAG laser for ∼5 μs. In this way, the CCD camera can record the very beginning of

*skocic@ff.bg.ac.rs

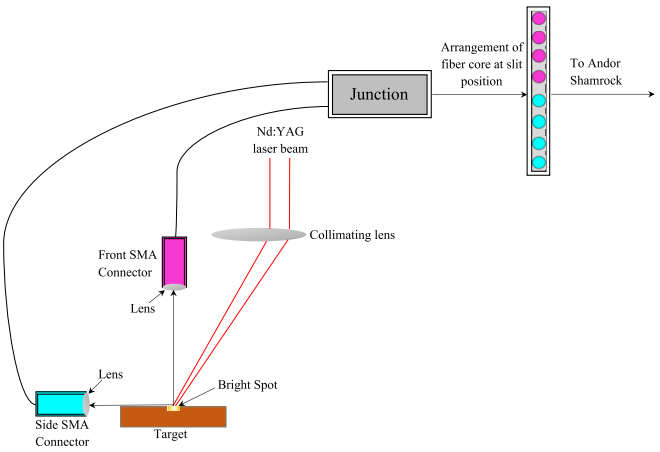

FIG. 1. Experimental Setup: The target is illuminated by the 1064 nm Nd:YAG harmonic. The bright area is monitored by two legs of the bifurcated optical cable equipped with identical SMA collecting lenses focused on the hot spot. At the common end of the cable the fiber cores are arranged in line providing simultaneous detection on the camera CCD.

the heating of the metal surface when the intensity of the laser is far below its maximum intensity.

III. MEASUREMENT PROCEDURE

There are two key points in the measurement process: the identification of the emitted light source and how to apply the calibration procedure. As it is explained, use of the bifurcated optical cable provides simultaneous registration of the spectra

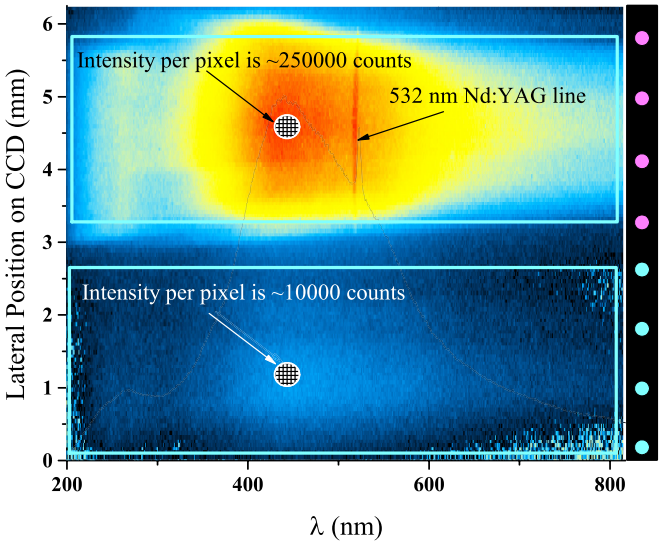

FIG. 2. The image captured by CCD. The upper part of the image is illuminated by fiber cores coming from the upper leg of the cable (front lens), while lower part is illuminated by fiber cores from the lower leg (side-on lens). The regular spectra are subsequently extracted from the image (rectangular areas indicated on image) with a special attention to avoid overlapping. The color code is logarithmic to make intensities from the lower lag visible. The irradiance at the target surface was 3.2×10^{11} W/cm^2. Delay was $\tau = 16$ ns while exposure time was set to 1 ns.

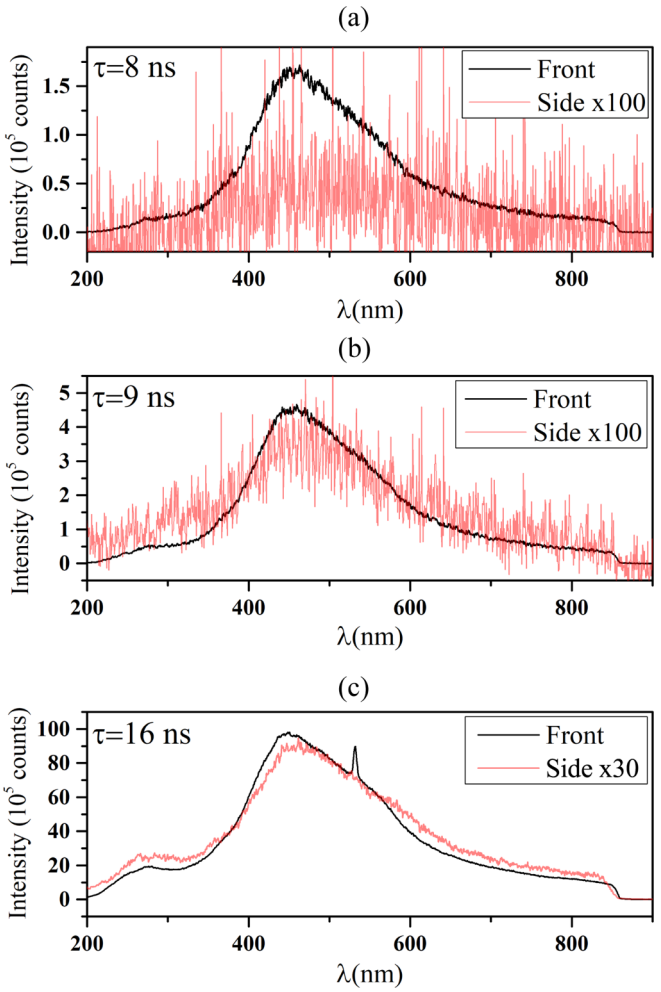

FIG. 3. Spectra captured by the front collecting lens (black line) and side-on (red line). The original intensities collected side-on are significantly lower than corresponding intensities recorded by the front lens, therefore side-on spectra are multiplied by factor 100 (a, b) and 30 (c), to make their profiles visible. It is easily seen that at the very beginning of the laser action (a) the light, dominantly emitted by the hot metallic surface, is captured only by the front lens, while at the late moment (c) both spectra are very similar, signifying that both lenses capture light from the same source, plasma expanding above the target surface. At 9 ns (b), the intensity captured side-on is very low but has essentially the same shape as the intensity recorded by the front lens indicating that before 9 ns source of radiation is dominantly hot metallic surface. The irradiance at the target surface was 3.2×10^{11} W/cm^2. The peak at 532 nm (c) is caused by leakage of the first Nd:YAG harmonic.

captured side-on and captured by the front collecting lens. At the very beginning, when the laser pulse starts to heat-up the metallic target, the front collecting lens will collect light without any limitation, while the side-on lens, due to an unfavorable viewing angle, will collect mostly the stray light of the very low intensity. It is quite difficult to identify the position, even the existence, of the plasma at that moment. Continuous spectrum recorded by the front lens is dominantly determined by the temperature of the hot metallic target. Plasma, when created, starts to expand and light emitted by the plasma becomes visible for the "side-on" lens (Fig. 3). Comparing

intensities and spectral shapes (temperatures) collected by both lenses one can estimate whether the bright spot is due to hot metallic surface or light emission originates from the plasma which radiates nearly as black body.

The radiometric calibration is conducted for both legs of the bifurcated optical cable. With $C(\lambda)$ we denote calibration curve which is related to recorded spectrum $I_r(\lambda)$ and emitted spectrum $I_e(\lambda)$ in the following way: $I_r(\lambda) = I_e(\lambda)C(\lambda)$. It follows that

$$I_e(\lambda) = I_r(\lambda)/C(\lambda). \tag{1}$$

Comparing $I_e(\lambda)$ with black-body spectrum characterized by Planck's relation $I_P(\lambda, T)$[1] one can estimate temperature of the emitter. However, due to noise present in $I_r(\lambda)$ and $C(\lambda)$ the ratio $I_r(\lambda)/C(\lambda)$ is for some recordings prone to large scatter at the end of intervals making fitting procedure inaccurate.

A simple way to overcome this difficulty is to multiply Planck's spectrum by the calibration curve

$$I_P(\lambda, T)C(\lambda) \tag{2}$$

and compare it, in sense of the least-square method, with recorded spectrum $I_r(\lambda)$; see Fig. 4. This approach is in some cases numerically more stable. It is difficult to adopt any formal error estimation procedure as an adequate measure for uncertainty in the evaluated temperature. Supposing that experimental data and calibration curve are free of systematic errors, uncertainty of the temperature reported by the correctly weighted[2] least-square method is unrealistically low, only a few hundred kelvins. On the other side, possible systematic errors in the calibration curve and recorded data are spread over the spectrum and both are difficult to identify. To take into account impact introduced by possible presence of systematic errors we applied calibration curve $C(\lambda)$ in different ways in Eqs. (1) and (2) and adopted inconsistency in temperature, reported by both fitting procedures, as a reasonable estimate of the accuracy achieved in the experiment. In this manner uncertainty associated to temperature is more realistic, about 1000 K, depending on specific data set.

For temperatures above 15 000 K, according to Planck's law, maximum of emission is in the UV part of the spectrum, at wavelengths below the detection range of the setup. In this case the fitting procedure relies only on the points from the "red wing" of Planck's curve, resulting generally in lower accuracy. Typical values of the relative errors associated to the temperature are $\lessapprox 20\%$.

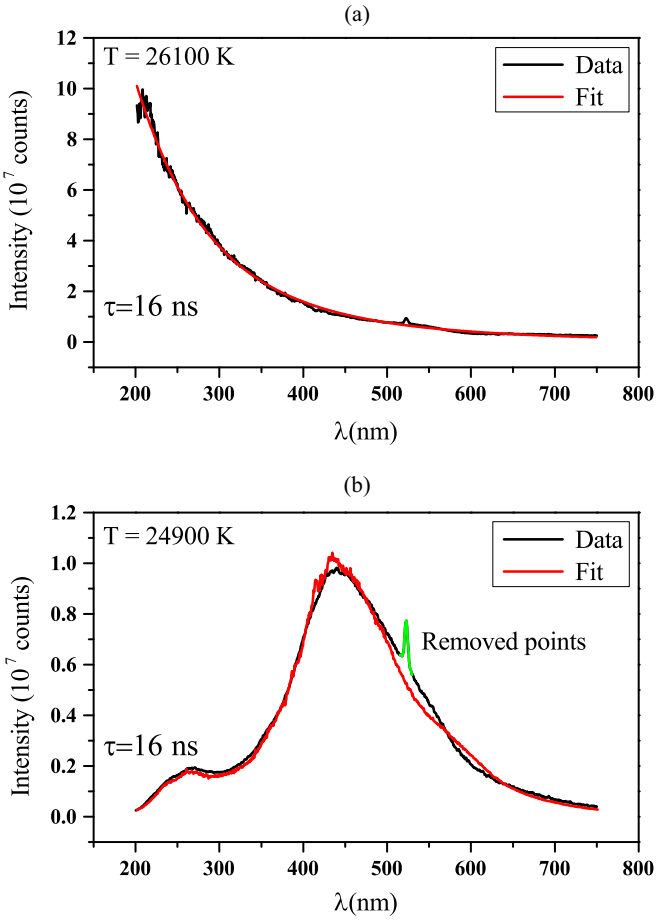

FIG. 4. (a) The radiometric calibration curve $C(\lambda)$ is applied on the recorded spectrum $I_r(\lambda)$ to reproduce emitted spectrum I_e in the following way $I_e(\lambda) = I_r(\lambda)/C(\lambda)$. The best fit curve is obtained by minimizing $\sum_\lambda [I_e(\lambda) - I_P(\lambda, T)]^2$ where T is a temperature, the only fit parameter. (b) The calibration curve is applied on Planck's theoretical spectrum, $I_P(\lambda, T)C(\lambda)$. This quantity can be directly compared with recorded spectrum $I_r(\lambda)$ while temperature T, the only fit parameter, is evaluated by minimizing $\sum_\lambda [I_r(\lambda) - I_P(\lambda, T)C(\lambda)]^2$. The irradiance at the target surface was 3.2×10^{11} W/cm^2. The spectrum is captured by the front collecting lens. Note that, in spite of imperfection of the fit in panel b, the deduced temperatures match within ≈5%.

IV. RESULTS

Figure 5 summarizes our experimental findings. The black arrows indicate moments when both collecting lenses start to capture measurable amounts of light of nearly the same (continuous) spectral shape. This result suggests that both lenses collect the light coming from the same source, the plasma formed above the metallic surface. Therefore, the temperature evaluated from the spectral shape is dominantly attributed to plasma. In recordings made 2 ns earlier,[3] the "side-on" collecting lens captures just a stray light of minimal intensity, while the light captured by the front lens has a regular

[1] $I_P(\lambda, T) = \frac{A}{\lambda^5[\exp(\frac{hc}{\lambda kT})-1]}$, where A is a fitting constant, h is Planck's constant, c is speed of light, k is Boltzmann's constant, λ is wavelength, and T is temperature.

[2] Uncertainty of every point $I_e(\lambda)$ is calculated applying error propagation procedure according to Eq. (1), i.e., $\frac{\Delta I_e(\lambda)}{I_e(\lambda)} = \sqrt{[\frac{\Delta I_r(\lambda)}{I_r(\lambda)}]^2 + [\frac{\Delta C(\lambda)}{C(\lambda)}]^2}$, where $[\frac{\Delta I_r(\lambda)}{I_r(\lambda)}] \sim \frac{1}{\sqrt{n}}$, while n is intensity in counts measured by CCD camera. Due to averaging of successive spectra, n is a large number. Therefore, the relative error $\frac{1}{\sqrt{n}}$ is less than 1% for $n > 10^5$. $\frac{\Delta C(\lambda)}{C(\lambda)}$ is claimed, by Stellar net, to be also below 1%. We adopted for $\frac{\Delta I_e(\lambda)}{I_e(\lambda)}$ an overestimated value of 2% which for data in Fig. 4(a) results in less than 100 K uncertainty in temperature T estimated by the least-square method.

[3] We have chosen 2 ns to be certain that we capture the light coming just from the metallic surface.

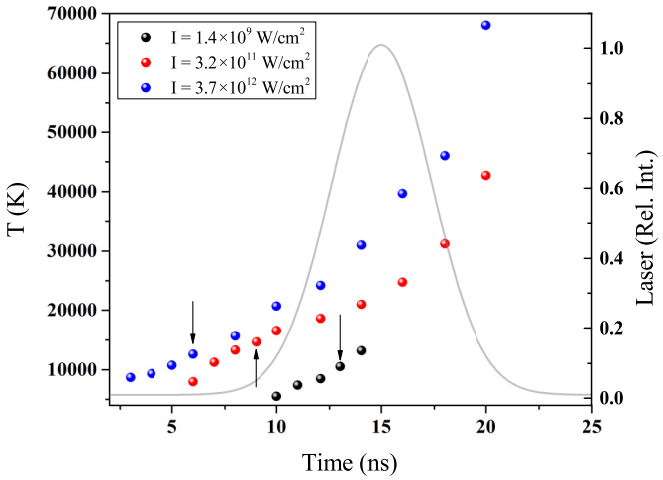

FIG. 5. Temperatures of the area illuminated by the laser, for three different irradiance, as a function of time. The gray curve is normalized temporal profile of the laser pulse. The black arrows indicate moments when side-on lens starts to collect light with spectrum similar to one captured by the front lens. Accuracy of the estimated temperatures is about 20%.

continuous spectrum. According to idea presented in Sec. III this finding is caused by unfavorable viewing angle of the "side-on" lens when the source of radiation is just the hot metallic surface. Hence, the temperature evaluated from the spectrum recorded by the front lens is dominantly attributed to metallic surface. The summary of results is presented in Table I.

One can see that the highest temperatures attributed to the metal are considerably high and even for the lowest applied irradiance (1.4×10^9 W/cm^2) the temperature of $\sim$ 7400 K is close to the most of estimates for copper critical temperature, see Demin *et al.* [12] and references therein. As it is expected the time needed to heat up the metal surface to its maximum temperature is inversely proportional to applied laser power. Keeping in mind that accuracies are about 20% it follows that the highest temperatures attributed to the copper surface overlap to a significant extent (Table I). With the current experimental setup, we are not able to check whether the maximum copper temperature is essentially the same for the applied irradiances range or not. This findings are in general agreement with results for copper obtained by comprehensive simulations conducted for similar conditions, see Refs. [15,16].

After the moments indicated by the arrows, the measured temperatures are predominantly attributed to the plasma formed above the copper surface. As we mentioned, for temperatures above 15 000 K, maximum of the light emission is in UV region so that fitting procedure is less reliable and error margins are over 20%. Nevertheless, for irradiances of 3.2×10^{11} W/cm^2 and 3.7×10^{12} W/cm^2 the evaluated temperatures are above 30 000 K. For delays of 15–20 ns the absorption of 1064 nm harmonic in the plasma attains its maximum, see Dojić *et al.* [3], so it is not surprising that in these moments the temperature reaches high values. Again, these temperatures are in reasonable agreement with results for copper obtained by simulation [15].

TABLE I. The highest temperatures that can still be attributed to the metallic surface. Values for ΔT are 20% fraction of the presented temperature.

Irrad. (W/cm^2)	T (K)	ΔT (K)	Delay (ns)
1.4×10^9	7400	1500	11
3.2×10^{11}	11 200	2200	7
3.7×10^{12}	9300	1900	4

V. TEMPORAL EVOLUTION AND TEMPERATURE RELAXATION IN THE PLASMA

Immediately after the laser is triggered, recorded spectra are continuous with the shape very similar to black-body radiation. Couple of nanoseconds later, depending on applied irradiance, the spectral lines appear indicating that plasma rarefy and departs from thermal equilibrium. In Fig. 6 we present color-coded 2D graph of the recorded spectra from 10th ns for irradiance of 1.4×10^9 W/cm^2 and from the 6th ns for irradiance of 3.2×10^{11} W/cm^2. One can see that for lower irradiance, Fig. 6(a), the spectral lines appear starting from 15th ns. After that moment temperature cannot be estimated from Planck's relation [17]. However, for irradiance of 3.2×10^{11} W/cm^2, Fig. 6(b), the plasma emits only continuous spectrum during the laser pulse. All our measurements are restricted to the intervals of the time when spectrum of the plasma is strictly continuous; see Fig. 5.

Regardless of the fact that recorded spectra are to the large extent continuous, we will provide a rough estimate of the temperature relaxation time between free electrons and ions. Namely, during the laser pulse energy of electromagnetic radiation is predominantly absorbed by free electrons and subsequently, in numerous collisions, transfers to heavy particles—ions and atoms. Depending on plasma parameters collision rate changes, and therefore changes the temperature relaxation time t_r too. To be able to correctly characterize the plasma with a single temperature, t_r should be sufficiently short to keep electron temperature T_e and temperature of ions T_i on the nearly the same value despite the process of heating the electrons by the laser. Having in the mind that the laser intensity changes significantly on one nanosecond scale and that the exposure time is 1 ns we can conclude that t_r should be less than 1 ns.

The temperature relaxation time, for the actual problem, according to Spitzer [18], is

$$t_r = (4\pi\varepsilon_0)^2 \frac{3 m_e m_i k^{3/2}}{8\sqrt{2\pi} n_i Z_i^2 e^4 \ln\Lambda} \left(\frac{T_e}{m_e} + \frac{T_i}{m_i} \right)^{3/2}, \qquad (3)$$

where ε_0 is vacuum permittivity, m_e and m_i are mass of electron and copper ion, respectively, k is Boltzmann constant, n_i is density of the ions, Z_i is charge of the actual ionization state, e is electron charge, while T_e and T_i are electron and ion temperatures, respectively. The ln Λ is Coulomb logarithm.

While Eq. (3) is exact, estimation of Z_i, n_i, T_e, and T_i is a difficult task. Instead of comprehensive simulation we will rely on a choice of the most unfavorable values for Z_i, n_i, T_e,

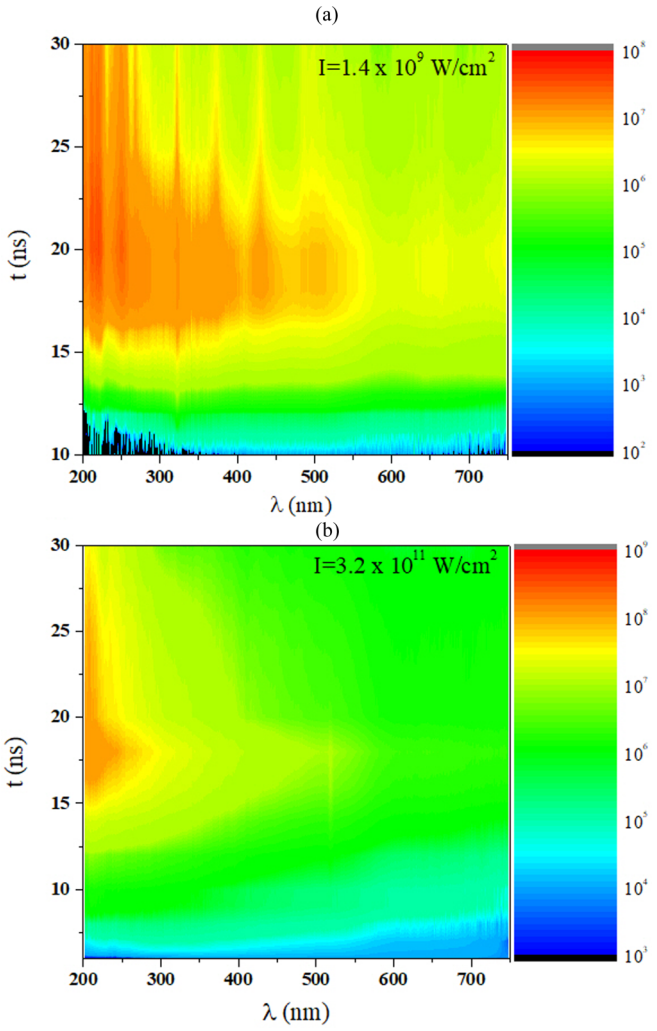

FIG. 6. Temporal evolution of the copper spectrum during the laser pulse for two irradiances, $I = 1.4 \times 10^9$ W/cm^2 (a) and $I = 3.2 \times 10^{11}$ W/cm^2 (b). Intensity of the radiation, $P(\lambda, t)$, is presented by color code. It is evident that after 15 ns, for lower irradiance (a), the continuous spectrum is gradually transformed into a line spectrum despite the action of the laser. For higher irradiance spectrum remains continuous during the laser pulse.

and T_i in respect to the temperature relaxation time t_r. One can see that t_r is very sensitive on ionization states present in the plasma due to Z^2 term in denominator. Accordingly, we assume that plasma is fully ionized but only ions with Z_i=1 are present. We adopted n_i to be about two orders of magnitude less than concentration of atoms/ions in metallic copper, i.e., $n_i = n_e \approx (10^{26}$–$10^{27})$ m^{-1}. Temperature of the electrons, due to heating by the laser, is taken to be in the interval $T_e \approx$ (50 000–100 000) K, while T_i is kept on 6000 K.

The temperature relaxation time attains value t_r= 2 ns for the highest electron temperature $T_e = 10^5$ K and for the lowest ion density $n_i = n_e$=10^{26} m^{-3}. If the electron temperature is T_e = 50 000 K and $n_i = n_e = 10^{27}$ m^{-3} the relaxation time is satisfactorily low, i.e., $t_r = 0.37$ ns. For the electron temperatures above 50 000 K in the copper plasma, according to Saha equation, dominant particles are Cu^{++} and Cu^{+++} ions with $Z_i = 2$ and 3. Large Z in denominator of Eq. (3) reduces additionally t_r making it less than 1 ns. We can conclude that during the laser pulse both temperatures, T_e and T_i, are reasonably close to each other and can be approximated by the single temperature T derived from the continuous spectra inherent for the plasma at this stage of development.

Furthermore, the rate coefficient for the collisional excitation to the first excited level of the resonance series as the slowest one can serve as the base for a rough estimate of relaxation time among the internal electronic degrees of freedom via inelastic collisions. For the above-mentioned temperature and density range, according to Ref. [19] this value is below 10^{-11} s.

VI. CONCLUSION

In this work we present a technique for measurement of copper surface temperature at the very beginning of the laser-induced breakdown experiment, before creation of the plasma. The experiment is conducted by Nd:YAG laser for three irradiances: 1.4×10^9, 3.2×10^{11}, and 3.7×10^{12} W/cm^2 at the residual atmosphere of 0.05 mbar. It is found that temperature of the copper surface is in the interval 7 400–11 200 K. These values are close to the most data available in the literature for the critical temperature of the copper. We estimated that the relaxation time of electron and ion temperature necessary to achieve equilibrium via elastic collisions is less than 1 ns. Also, the relaxation time among the internal electronic degrees of freedom via inelastic collisions is estimated to be below 10^{-11} s.

ACKNOWLEDGMENTS

This work is part of Project No. 451-03-9/2021-14/200162 supported by the Ministry of Education, Science, and Technological Development of the Republic of Serbia.

[1] A. Bogaerts and Z. Chen, Effects of laser parameters on laser ablation and laser-induced plasma formation: A numerical modeling investigation, Spectrochim. Acta B: Atom. Spectrosc. **60**, 1280 (2005).

[2] A. H. A Lutey, An improved model for nanosecond pulsed laser ablation of metals, J. Appl. Phys. **114**, 083108 (2013).

[3] D. Dojic, M. Skocic, and S. Bukvic, Shielding effects in interaction of nanosecond laser pulses with solid target, Spectrochim. Acta B: Atom. Spectrosc. **186**, 106319 (2021).

[4] A. Bataller, G. R. Plateau, B. Kappus, and S. Putterman, Black-Body Emission from Laser Breakdown in High-Pressure Gases, Phys. Rev. Lett. **113**, 075001 (2014).

[5] M. M. Martynyuk, Phase explosion of a metastable fluid, Combust. Explos. Shock Waves **13**, 178 (1977).

[6] A. Miotello and R. Kelly, Laser-induced phase explosion: New physical problems when a condensed phase approaches the thermodynamic critical temperature, Appl. Phys. A: Mater. Sci. Process. **69**, S67 (1999).

[7] N. M. Bulgakova and A. V. Bulgakov, Pulsed laser ablation of solids: Transition from normal vaporization to phase explosion, Appl. Phys. A **73**, 199 (2001).

[8] Q. Lu, Thermodynamic evolution of phase explosion during high-power nanosecond laser ablation, Phys. Rev. E **67**, 016410 (2003).

[9] A. A. Ionin, S. I. Kudryashov, and L. V. Seleznev, Near-critical phase explosion promoting breakdown plasma ignition during laser ablation of graphite, Phys. Rev. E **82**, 016404 (2010).

[10] A. L. Horvath, Critical temperature of elements and the periodic system, J. Chem. Educ. **50**, 335 (1973).

[11] J. A. Cahill and A. D. Kirshenbaum, The density of liquid copper from its melting point (1356 K) to 2500 K and an estimate of its critical constants, J. Phys. Chem. **66**, 1080 (1962).

[12] M. M. Demin, O. N. Koroleva, A. V. Shapranov, and A. A. Aleksashkina, Atomistic modeling of the critical region of copper using a liquid-vapor coexistence curve, Mathematica Montisnigri **46**, 61 (2019).

[13] M. Skočić and S. Bukvic, Laser induced plasma expansion and existence of local thermodynamic equilibrium, Spectrochim. Acta B: Atom. Spectrosc. **125**, 103 (2016).

[14] D. Bleiner and A. Bogaerts, Laser-induced plasmas from the ablation of metallic targets: The problem of the onset temperature, and insights on the expansion dynamics, J. Appl. Phys. **101**, 083301 (2007).

[15] A. Bogaerts, Z. Chen, R. Gijbels, and A. Vertes, Laser ablation for analytical sampling: What can we learn from modeling? Spectrochim. Acta B: Atom. Spectrosc. **58**, 1867 (2003).

[16] D. Autrique, G. Clair, D. L'Hermite, V. Alexiades, A. Bogaerts, and B. Rethfeld, The role of mass removal mechanisms in the onset of ns-laser induced plasma formation, J. Appl. Phys. **114**, 023301 (2013).

[17] J. A. M. van der Mullen, Excitation equilibria in plasmas: A classification, Phys. Rep. **191**, 109 (1990).

[18] L. Spitzer, *Physics of Fully Ionized Gases* (Interscience, New York, NY, 1956).

[19] G. Cristoforetti, A. De Giacomo, M. Dell'Aglio, S. Legnaioli, E. Tognoni, V. Palleschi, and N. Omenetto, Local thermodynamic equilibrium in laser-induced breakdown spectroscopy: Beyond the McWhirter criterion, Spectrochim. Acta B: Atom. Spectrosc. **65**, 86 (2010).